Seismic tomography of Central São Miguel, Azores

Daria Zandomeneghi [a,1], Javier Almendros [a,b,*],
Jesús M. Ibáñez [a,b], Gilberto Saccorotti [c,2]

[a] *Instituto Andaluz de Geofísica, Universidad de Granada, Campus de Cartuja, 18071 Granada, Spain*
[b] *Departamento de Física Teórica y del Cosmos, Universidad de Granada, Campus de Fuentenueva, 18071 Granada, Spain*
[c] *Istituto Nazionale di Geofisica e Vulcanologia (INGV)-Osservatorio Vesuviano, Via Diocleziano 328, 80124 Napoli, Italy*

A B S T R A C T

We determine the three-dimensional distribution of P- and S-wave velocities for Central São Miguel Island (Azores, Portugal) by tomographic inversion of local earthquake arrival times. We use P- and S-phases from 289 earthquakes recorded by a network of 20 seismometers. The model shows good resolution in the shallowest 5–6 km, as illustrated by different resolution tests. There are several velocity anomalies, interpreted as pyroclastic deposits, intrusive bodies, geothermal fields, and the effects of tectonics. A low Vp zone marks Furnas caldera, probably evidencing volcaniclastic sediments with development of intense geothermal activity. Another low Vp zone extends in correspondence of the highly fractured area between Fogo and the north coast. Conversely, strong positive anomalies are found south of Fogo and northwest of Furnas. They are interpreted in terms of high-density deposits and remnants of a plutonic intrusion. These interpretations are supported by the distribution of Vp/Vs, and are consistent with previous geological, geochemical, and geophysical data.

© 2008 Elsevier B.V. All rights reserved.

1. Introduction

The Archipelago of Azores consists of nine volcanic islands located at about 38°N–28°W, in the triple junction zone among the American, Eurasian, and African plates. The largest island is São Miguel (Fig. 1). The structure of São Miguel is characterized by fault systems mainly trending NW-SE and E-W. The most important volcanic complexes are located at the intersection of these tectonic lineaments (see Cruz, 2003 and references therein). In Central São Miguel, the main volcanic structures are those of Fogo and Furnas. Both are central volcanoes with a summit caldera and a dominantly trachytic composition. Furnas is the youngest volcano and consists of a steep-sided, 8 km ×5 km caldera complex formed during several collapses (Guest et al., 1999). In the last 3000 years, most eruptions were phreato-magmatic and occurred with an average recurrence interval of 320 years (Moore et al., 2001). The Fogo volcanic edifice rises to an elevation of ∼ 1000 m above sea level, and is composed by lava flows, domes and pyroclastic deposits over an older submarine lava basement. See, for example, Guest et al. (1999) for a detailed description of the geology of the area.

Although Central São Miguel volcanoes have not erupted since the 17th century, the area is restless. Geothermal manifestations are conspicuous and constitute one of the most important present day indications of volcanism. Geothermal exploration and research evidence two main active fields, in the Ribeira Grande-Fogo and Furnas regions. In these fields, local tectonics seem to control subsurface flow and the alignment of fumaroles and thermal springs (Ferreira and Oskarsson, 1999). The most intense thermal activity coincides with an E-W tectonic lineament in Furnas and a NW-SE fault system in Fogo (Cruz, 2003). At Ribeira Grande, the geothermal field is possibly connected to a reservoir between Fogo and the northern coast, hosted by highly fractured, pyroclastic rocks (Muecke et al., 1974; Gandino et al., 1985; Carvalho et al., 2006). The heat source, especially for deeper levels of the field, could be a regional heat anomaly (Silveira et al., 2006; Ritsema and Allen, 2003). At Furnas, the heat source is probably the plutonic remnants of the most recent volcanism below the center of the caldera, although there are no clear signs of direct magmatic contribution in the discharge composition (Cruz et al., 1999).

To study the structure related to the volcanic activity of the island, several investigations have been carried out. Camacho et al. (1997) performed a gravimetric study of São Miguel island to determine the density distribution in the first kilometers. At depths

* Corresponding author at: Instituto Andaluz de Geofísica, Universidad de Granada, Campus de Cartuja s/n, 18071 Granada, Spain. Tel.: +34 958 249552; fax: +34 958 160907.
E-mail address: alm@iag.ugr.es (J. Almendros).
[1] Now at New Mexico Tech-801 Leroy Place, Socorro, NM 87801, USA.
[2] Now at INGV-Sez. di Pisa, Via U. della Faggiola 32, 56126 Pisa, Italy.
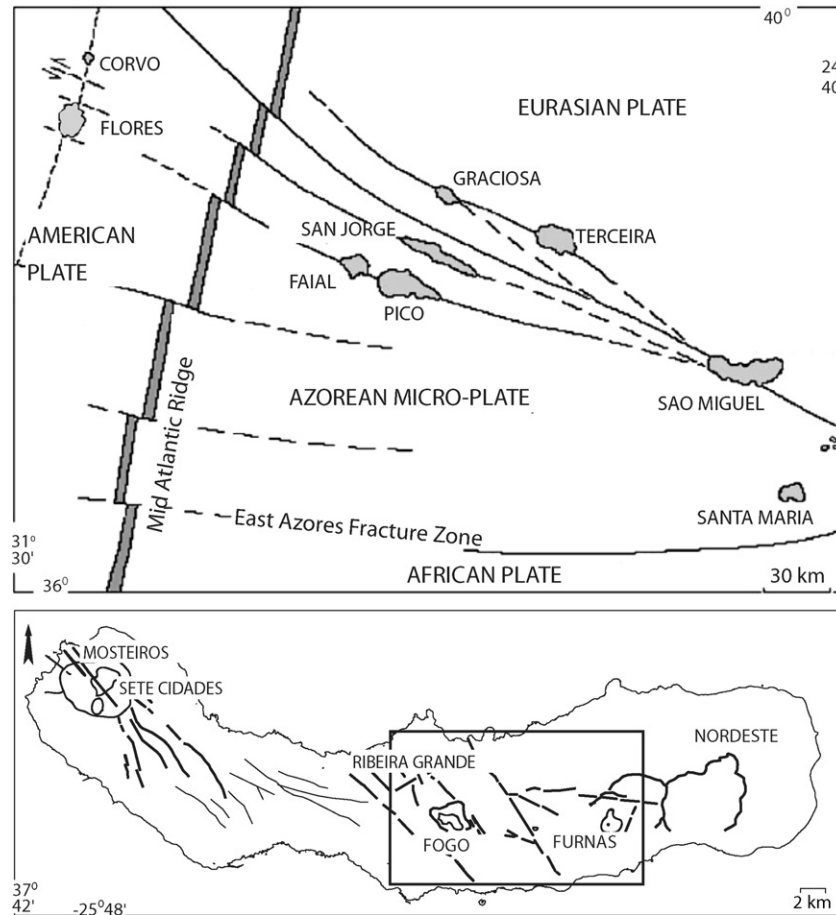
Fig. 1. (Top) Regional map showing the location and main tectonic features of the Azores Archipelago. (Bottom) São Miguel map with names of the most prominent regions. The box corresponds to the area selected for the study.

around 8 km, the areas around Fogo and Furnas show two density minima separated, in Congro zone, by a high-density region that shows a NE-SW trend. It extends to shallow depths (still present at 1 km) and has been interpreted as an old basaltic shield or a partly solidified magmatic body. Montesinos et al. (1999) focused on the gravimetric low-density anomaly of Furnas area. At shallow levels, this anomaly is interpreted as low-density silicic caldera infill, mainly due to collapse processes, and volcanic products from several eruptions which occurred after the formation of the main caldera from radial and concentric fractures. Deformation and GPS measurements performed at Central São Miguel have revealed a slight inflation of the Furnas area (Sigmundsson et al., 1995). An explanation refers to the presence of fluids within a deep hydrothermal system beneath the caldera, sealed by an impermeable zone and forced to growing pressures. At Fogo, GPS stations show displacements toward the caldera, indicating a slight deflation of the volcano (Jónsson et al., 1999). This deflation could be due to a pressure decrease in the magma chamber, or to the extraction of water and steam by a nearby geothermal power plant.

In the last years, thousands of earthquakes have been annually recorded and located around São Miguel island by the regional seismic network. Their origin is mostly related to the approximately WNW-ESE fault systems dominating the regional tectonics (e.g. Udías et al., 1976; Madeira and Ribeiro, 1990). Central São Miguel is crossed by different fault systems, trending NW-SE and E-W, and constitutes one of the most active seismogenic regions in the Azores (e.g. Gongora et al., 2004; Escuer, 2006). This observation is compatible with the focal mechanisms calculated in the area (Udías et al., 1976; Buforn et al., 1988) and the strike-slip faulting observed in the bathymetry (Lourenço et al., 1998).

The local seismic network evidences that a substantial number of the earthquakes are swarms of local, low-magnitude earthquakes located in the area between Fogo and Furnas (D. Silveira, personal communication). Although the tectonic control seems important, a recent work by Luis (2006) suggests that these swarms are not generated by a tectonic-driven mainshock/aftershock mechanism. The most likely explanation is that Central São Miguel earthquake swarms have a volcano-tectonic origin.

Inhabited volcanic areas, where even a small eruption could produce considerable losses, pose important problems in terms of hazards. This consideration motivated an European Union-sponsored project (named *e-Ruption*) intended to quantify the present-day seismicity of various quiescent volcanoes in populated regions (Saccorotti et al., 2004). One of the selected sites was Central São Miguel, where a seismic survey was carried out in April–July 2003. In this paper, seismic data recorded in that experiment are used to determine the three-dimensional (3D) velocity structure of the central region of São Miguel. This work represents a first attempt to establish the relationship between seismic velocity distribution and volcanic structures in São Miguel Island.

2. Instruments and data

Between April 4 and July 15, 2003, a temporary network including short-period and broad-band instruments, as well as three small-aperture seismic antennas, was deployed in São Miguel
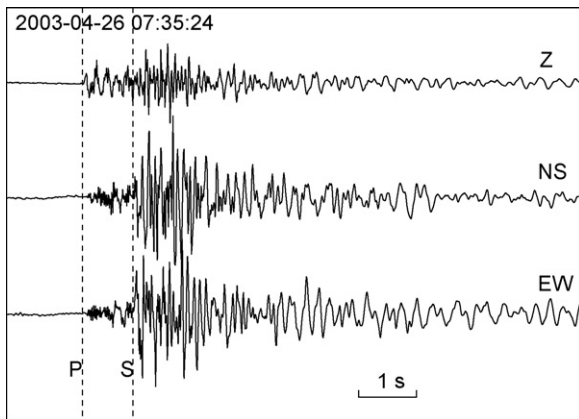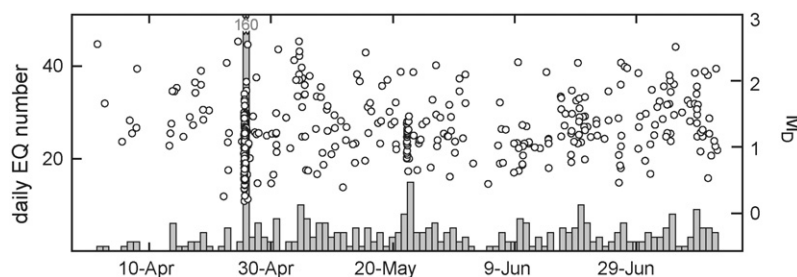
Fig. 2. Example of raw seismograms recorded by a short period, three-component station during the Central São Miguel experiment. Starting time of record and P- and S-phase arrivals are also indicated.

Fig. 4. P-wave velocity model used in routine network locations (light gray line, TAC Model) and 1D model derived from our data (black line, minimum 1D Model) from 0 to 10 km depth.

(Saccorotti et al., 2004) to expand and complete the permanent network operated by "Sistema de Vigilancia Sismologica dos Açores" (SIVISA). During this period, our instruments recorded more than 1000 earthquakes. Most of them were local earthquakes (Fig. 2) characterized by S-P times smaller than a few seconds and with magnitude-durations lower than 2.5. The daily average was 5–10 earthquakes per day, except for a single swarm in April 26–27 when more than 160 earthquakes occurred in a few hours (Fig. 3).
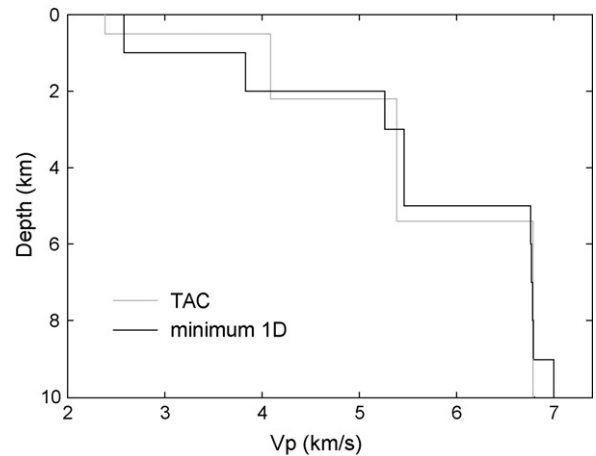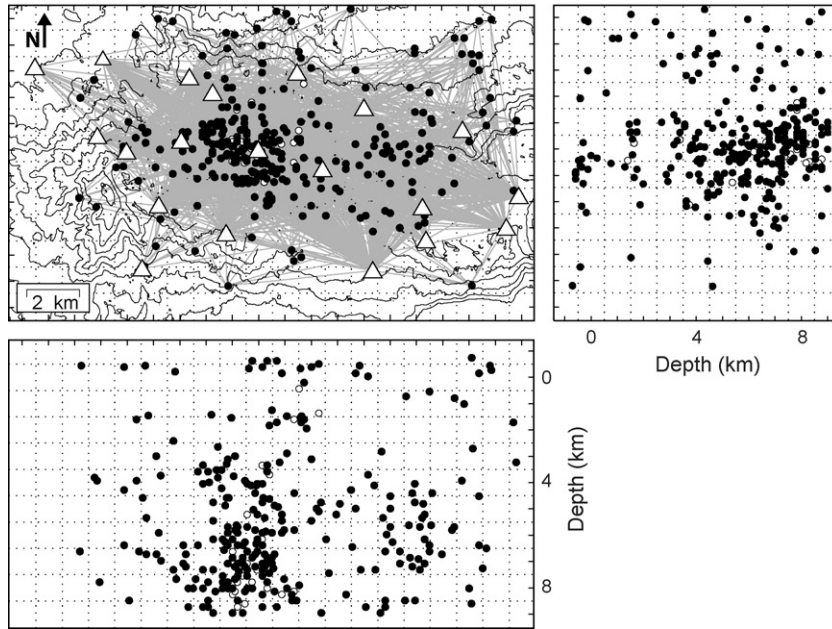
Our starting dataset consisted of visually picked arrival times for P- and S-phases associated with 426 earthquakes, recorded in a seismic network of 26 stations (Fig. 1). They mostly had a time difference between arrivals of P- and S-waves smaller than 3 s, and were hence considered as local earthquakes.

3. Method

We chose the seismic tomography code of Benz et al. (1996) to calculate the 3D velocity structure of Central São Miguel. This method is particularly appropriate for the study of volcanic areas, usually characterized by sharp velocity heterogeneities that can strongly affect seismic wave propagation. The method uses the finite difference technique of Podvin and Lecomte (1991) (later modified by Tryggvason and Bergman, 2006) to calculate travel times and allows for the simultaneous inversion of the 3D P-wave velocity structure and earthquake locations. For these reasons, it has been applied to investigate the interior of several volcanoes such as Redoubt (Benz et al., 1996), Etna (Villaseñor et al., 1998), Kilauea (Dawson et al., 1999) and Vesuvio (Scarpa et al., 2002), and calderas, for example, Campi Flegrei (Zollo et al., 2003).

3.1. Preliminary model

To apply this method to the São Miguel data, we need an initial guess for the velocity model of the region and preliminary earthquake locations. A preliminary 1D velocity model was obtained using the code *Velest* (Kissling et al., 1994), that determines the velocity structure where calculated travel times best fit the observed phase arrivals, in a least-square sense. To calculate our 1D model, we started with the "Terra Açores" (TAC) velocity model used in routine network locations by SIVISA (Escuer, 2006) and with a selection of 331 earthquakes with good quality of recorded signals. We tested several layering thicknesses and more than 100 initial models differing a random 10% with respect to the TAC model. We obtained a 1D model which slightly differed from the TAC model, mostly in the first 5 km of depth (Fig. 4). In the calculated 1D model, the rms reduced from 0.044 to 0.018 s. The average displacement for the earthquake locations was 0.02 and 0.07 km in horizontal and vertical directions, respectively.

Preliminary hypocenter locations for 426 earthquakes in the whole São Miguel area were then obtained with the location algorithm *Nonlinloc* (Lomax et al., 2000), which provides a maximum-likelihood solution for the source location problem. Arrival times were weighted according to their picking uncertainty. Quality levels of 0–4 were assigned, respectively, to time errors < 0.02, 0.02–0.05, 0.05–0.1, 0.1–0.2, and > 0.2 s. We found that most earthquakes are located in Central São Miguel, between Fogo and Furnas calderas, in the shallowest 10 km (Fig. 5).

Fig. 3. Histogram of the daily number of earthquakes recorded by the temporary network during the 2003 seismic experiment at São Miguel. In the same plot, we show magnitude-duration values (M_D) for those events.

Fig. 5. Stations (triangles) and earthquakes (black circles) used for the 3D inversion, projected on the horizontal plane and N-S and W-E vertical planes. P-wave ray paths (gray lines) and unused earthquakes (white circles) are also indicated. Grid parameterization (dotted lines) and 100-m topography contours are represented.

3.2. 3D Model

For the 3D velocity inversion, we selected 289 earthquakes with a minimum of six phase readings, a maximum station gap of 180°, a maximum offset between stations and earthquakes of 20 km, and a minimum distance between hypocenters of 0.4 km. A 20 km × 12 km × 11 km volume centered at 25.426°W and 37.774°N, extending from 1.5 km above sea level to a depth of 9.5 km, was selected for the tomographic inversion. The final database consisted of 2197 P-wave and 1786 S-wave travel times, recorded at 20 stations (14 short-period and 6 broad-band seismometers) located within the selected area. Taking into account the station and hypocenter distributions, we estimate that the central region of São Miguel is densely sampled by seismic rays to a depth of 7 km. The volume was parameterized with a grid of constant-slowness cubic cells. After several tests with different cell sizes, we selected a 1-km cell as the optimum dimension for our inversion. It represented a good trade-off between travel time rms, model resolution, and ray coverage (Benz et al., 1996). A denser grid of 0.25 km, obtained by linear interpolation of the 1 km grid, was used in the direct problem to calculate arrival times with an accurate ray path tracing. Fig. 5 shows the area and inversion grid selected for the 3D tomography; the locations of the selected stations and hypocenters; and the ray path coverage.

The selection of the smoothing parameter was based on minimizing the final rms without introducing instabilities or increasing the model roughness due to modelling of the noise (Benz et al., 1996). Moreover, we observed that low smoothing results in a decrease of the number of ray paths that the model was able to adjust. The best balance between rms and number of rays was achieved for a smoothing value of 60 (Fig. 6). Convergence of the tomographic inversion to a stable solution was obtained after 10 iterations. Using the P and S travel time data and a Vp/Vs ratio of 1.68 derived for the same area (Saccorotti et al., 2004; Escuer, 2006), the method provides relocated hypocenters and a 3D P-wave velocity model for Central São Miguel (hereafter, the CSM model).

The inversion code does not allow for variations of the Vp/Vs ratio across the model. Therefore, we used an indirect approach to obtain the 3D Vp/Vs distribution. We separated the source location and velocity determination problems and estimated independent velocity models for P- and S-wave velocities. We assumed that the hypocenters were fixed at the locations determined by our final, full-dataset inversion. To make comparable the resulting velocity models, we selected only those earthquakes with both P- and S-wave travel times. Then, we performed two independent inversions for velocity: (1) we used the P-wave travel times to obtain the P-wave velocity model and (2) we used the S-wave travel times as first arrivals for the S-wave velocity model. The initial S-wave model is derived from the starting 1D velocity model for the P-wave and a Vp/Vs of 1.68. The Vp/Vs model is calculated as the ratio between the obtained P and S velocity models.
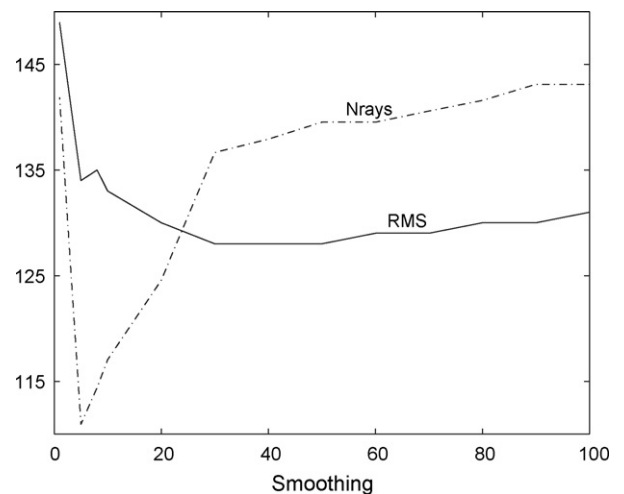
Fig. 6. Distribution of final rms and total number of used P-wave ray paths against smoothing values. The rms is indicated in ms. The ray number is divided by 15.
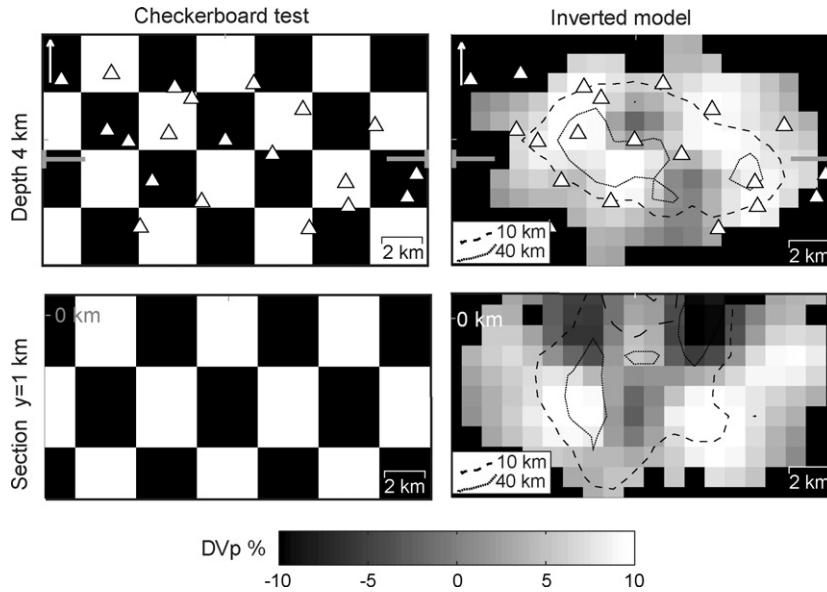
Fig. 7. Example of the results of a checkerboard test. Synthetic input model (left) and inverted model (right) for P-wave velocity. Map view (above) and W-E vertical section 1 km north of the map center (below). The contours indicate the total ray path length contained in each 1 km ×1 km ×1 km cell. Contours are shown for 20 and 40 km total ray length.

3.3. Resolution tests

The influence of systematic and random errors on the final results is hard to quantify owing to the nonlinear nature of seismic tomography, the difficulty of quantifying noise in the input data, and the effect of parameterization (Leveque et al., 1993; Calvert et al., 2000). A number of empirical methods of uncertainty estimation are used to ensure that only robust, well-constrained features of the final model are interpreted. They are based on the definition of artificial models with known distribution, dimension, and intensity of anomalies. The procedure presents two steps: first, we solve the direct problem to determine synthetic travel times and then we use those data as input for the inverse problem. The source–receiver geometry and inversion parameters have to be as close as possible to those used for the real data. The comparison of the final model with the initial (known) model provides a qualitative indication about the resolving capabilities. Regions where the recovered model closely matches the input model are considered well resolved. However, the degree of recovery is sensitive to the geometry and magnitude of the synthetic anomalies. These factors also have to be considered when interpreting the tests.

We defined synthetic models to perform checkerboard tests (Humphreys and Clayton, 1988) and impulse response tests (Ohmi and Lees, 1995). We also used the final velocity model to carry out a reconstruction test (Zhao et al., 1992; Barberi et al., 2004).

We built a checkerboard model characterized by alternated positive and negative anomalies of ±10% with respect to the initial 1D velocity model previously obtained. The anomaly dimensions were 3 km ×3 km ×4 km. In this model, with the same configuration of earthquakes and stations as in the real inversion, we calculated synthetic travel times. The 1D initial model was then used as starting velocity structure for the inversion of the synthetic database. In Fig. 7, we show results of the checkerboard test for a layer at 4 km depth and a E-W section at 1 km north of the center of the model. The best resolved areas are located in the center of the domain, to a depth of 5–6 km, in correspondence with largest ray path lengths and densely crisscrossed grid cells. Although, the anomaly pattern is well reproduced, the intensity is generally underestimated.

As the geometry of the checkerboard anomalies is very different with respect to the final velocity model, and the seismic ray paths as well, we figured out the resolution also in other anomaly distributions.

For the impulse response tests, we generated smoothed spot-like anomalies at different locations in the domain. These anomalies are well reproduced in the final models, specially those with high velocities. The resolved volume again coincides with the high-coverage area (Fig. 5), as in the checkerboard tests.

As an additional test, we calculated travel times in a velocity model equivalent to the CSM model. With this analysis we are able to check how well the inversion performs using anomalies with dimensions and positions similar to what we expect to deal with in the real medium. The parameter selection and inversion scheme were the same as in our 3D inversion. We added noise to the synthetic travel times in order to simulate the uncertainties in the real arrival time data. The noise level was inversely proportional to the quality assigned to the arrival time picks. To obtain a statistically robust estimate, this procedure was repeated to generate 25 noisy travel time datasets. When inverted, they generated a set of output models that show very slight differences among them. To compare the models, we used slowness rather than velocity because it shows a clearer Gaussian distribution of the final results. The standard deviations of slowness for each node are quite small, ranging between 1.1×10^{-3} and 8.7×10^{-3} s/km, with a mean value of 5.1×10^{-3} s/km. In Fig. 8, we compare the average reconstructed model and our final CSM model. We observe that the main features are well recovered, as in previous tests, until a depth of 5–6 km.

3.4. Input data tests

We assess the effects of the starting model and database characteristics. First, we performed the inversion using different trial structures as initial models. We perturbed the minimum 1D model by ±10% (Barberi et al., 2004), and calculated the corresponding P-wave velocity structures. The results of this test indicate that positions and shapes of the anomalies do not significantly change inside the studied volume.
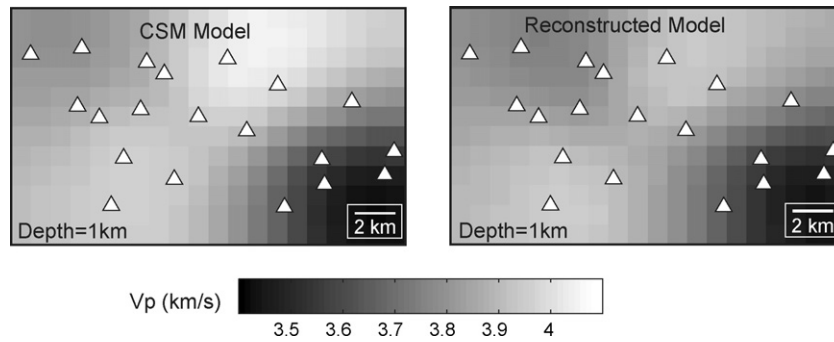
Fig. 8. Example of the results of the reconstruction test. Comparison between P-wave final CSM velocity model (left) and average model from 25 different reconstruction-test inversions (right). White triangles are seismic stations. Plots are horizontal sections at 1 km depth.

Next, we analyzed the control exerted on results by the database selection. We used a variation of the classical jackknife test, as suggested by Lees and Crosson (1989). A strong advantage of this method is that it does not require an estimate of noise in the data to assess the uncertainty in the resulting model because the noise itself contributes to the variance in the derived models. We performed 25 different inversions, removing a random 10% of the initial dataset, and then examining the variance of the derived models. The standard deviations among these models could be assumed as a measure of the uncertainty in the final model. Standard deviations for slowness among the final models were calculated at each node. They ranged from 0.2×10^{-3} to 2.6×10^{-3} s/km, with a spatially averaged value around 1.1×10^{-3} s/km. Comparing the average velocity model with the CSM model, we observe that the strongest differences occur at a few isolated points and are smaller than 6% of the averaged slowness at the same locations. From this point of view, the general framework of anomalies is not affected and main perturbations have a robust feature.

4. Results

Travel time data obtained during the 2003 experiment at São Miguel were inverted using the method described above. For P-phase arrival times, the average residual between observed and calculated values in the minimum 1D model was 0.35 s; in the final 3D model it was reduced to 0.13 s. For the S-phase, the rms reduction was from 0.44 to 0.15 s. This latter value refers to the inversion for the velocity model only. Earthquake locations changed an average of 0.09, 0.29, 0.25 km toward E, S, and depth. The origin times changed an average of 0.026 s.

The CSM model obtained contains several anomalous regions characterized by seismic velocities which differ from the starting values up to ∼ 10%. Fig. 9 shows the distribution of Vp and Vp/Vs in Central São Miguel. Those zones poorly resolved by the inversion, due to insufficient coverage, are shaded in gray. Several remarkable features appear in the seismic structure. We image a low-velocity anomaly in the Furnas zone, highly stable down to 6 km depth. The velocity values are over 10% lower than those of the starting model. Another zone of low velocity is situated in the NW corner of the studied area, between Fogo caldera and the north coast. This negative anomaly is weaker than the SE anomaly, and never surpasses the 2–3% value. Moreover, it stands in a peripheral region of our volume and for this reason it is pointed out by our resolution tests as tentative. This has to be taken into account in the interpretation step. On the contrary, the region extending from the south of Fogo to the northwest of Furnas, across the Congro area, shows clear positive anomalies, around 10% in their strongest values. This anomaly is actually constituted by two volumes, in the NE and SW extremes, separated by a slower zone. This zone has the highest ray coverage

and thus this partition in two sub-regions is probably a real feature of the velocity structure.

For the vertical distribution of heterogeneities, we observe that the overall positions of the model contrasts do not strongly vary with depth. The main anomalies stand in their positions, slightly changing in intensity. This means that whatever mechanisms produce the velocity variations, they extend all the way down to the depth resolved by our inversion. Fig. 10 shows interpolated vertical sections along two profiles (see Fig. 9) across the main anomalies. In this figure, we show the deep, poorly resolved levels as well, in order to understand the likely vertical extent of the anomalies. For example, the Furnas low-velocity anomaly extends in depth from 1 to 5 km, while the Ribeira Grande anomaly appears to be deeper. On the other hand, the northeastern high-velocity region deepens more than the southwestern high-velocity.

With respect to the Vp/Vs ratio of 1.68 previously derived for this area, both higher and lower values are retrieved by our inversion (Fig. 9). A central, high-ratio volume stands in the whole depth range. Between 1 and 5 km depth, high values extend eastward, closer to the Furnas area. Slightly high ratios appear between Fogo and the south coast. Low Vp/Vs can be observed in the north-northwest part of our volume and in the Furnas caldera zone. The lowest Vp/Vs ratios in both regions are found at about 2 km depth.

The Vp and Vp/Vs distributions contain features that do not overlap. For example, the SW and NE high velocity anomalies imaged in the Vp structure have completely different behavior in terms of Vp/Vs. The NE area has a low Vp/Vs ratio, while the SW region has a slightly high value around 1.7–1.8. This is an indication that these two anomalies are not related to the same processes, and underlines the need for Vp/Vs analysis when performing seismic tomography.

5. Discussion

From a seismological point of view, volcanic areas are complex structures. They exhibit solidified intrusions, partially molten regions, geothermally altered rocks, and intricate deposits of different shapes, thicknesses, and compositions. Therefore, volcanic regions are prone to enclose rocks with a wide range of physical properties (Foulger and Arnott, 1993). In seismological terms, this variability translates into the occurrence of strong contrasts of seismic wave velocity. The scenario is further complicated by the presence of fluids and structural discontinuities, definitely common in volcanic environments. Such factors usually affect Vp and Vs in different ways. Typically, the spatial variation of Vp mirrors the distribution of lithologies and rock properties, while the Vp/Vs ratio maps rock defects, pores, cracks, and their fluid content (Berge and Bonner, 2002). Since Vp and Vp/Vs are affected by different phenomena, both distributions have to be combined to envisage a global seismic structure.
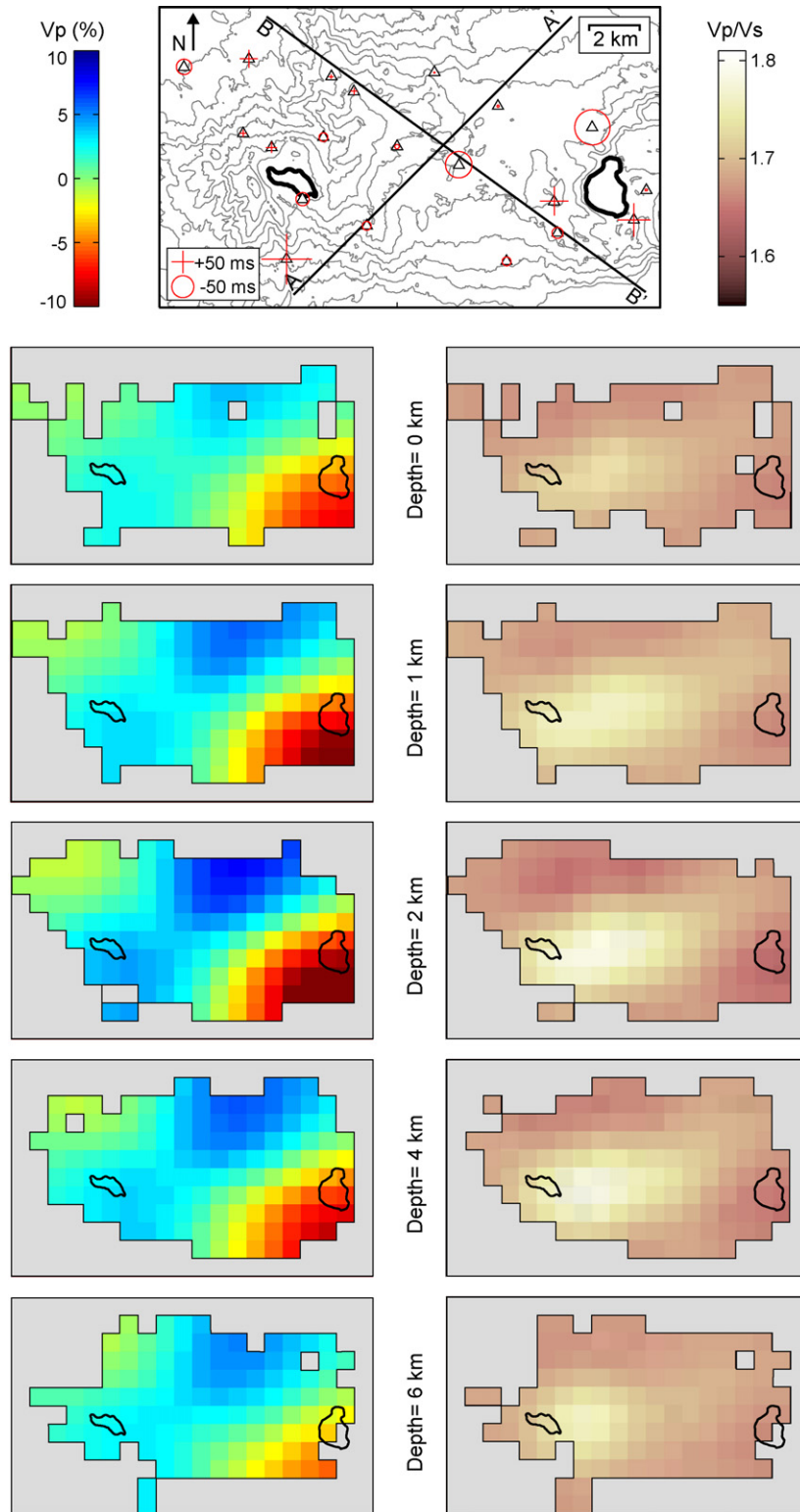
Fig. 9. Velocity model obtained from the tomographic inversion of P and S travel times (CSM model). (Top) Topographic map of CSM with 100-m contour lines. Triangles represent seismic stations. Red symbols indicate positive (cross) and negative (circles) station residuals. Fogo and Furnas lakes are marked with a bold line. Locations of A and B vertical sections (see Fig. 10) are also indicated. (Left) Horizontal sections of the P-wave velocity model at different depths, in % with respect to the initial model. (Right) Horizontal sections of the P- and S-wave velocity ratio. Unresolved areas are left as blank zones.

During the last decades, a wealth of studies has demonstrated that seismic tomography is a useful technique to investigate the structures of volcanic regions. Low-velocity anomalies interpreted as partially molten volumes have been found at Toba Caldera (Masturyono et al., 2001), Yellowstone (Husen et al., 2004), and Rabaul (Finlayson et al., 2003). Low-velocity regions have also been associated with geothermal systems (e.g. Coso geothermal system (Wu and Lees, 1999; Sanders et al., 1995)), and low-density caldera
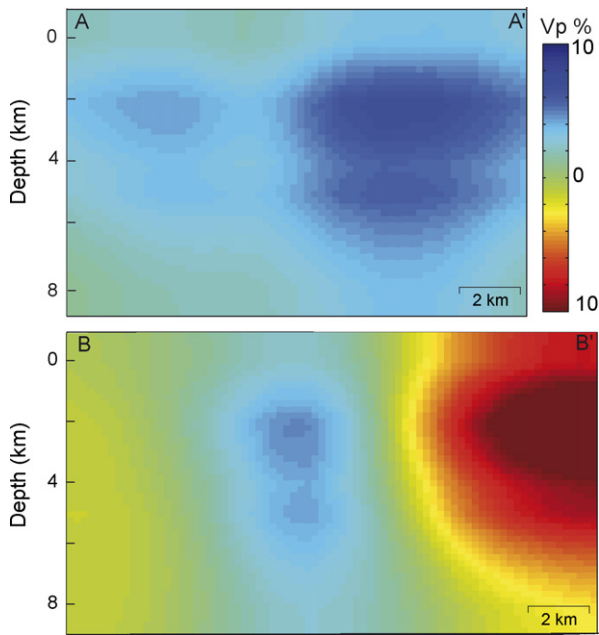
Fig. 10. Vertical sections of the final model along profiles A and B (see Fig. 9).

infilling materials (e.g. Taupo volcanic zone (Sherburn et al., 2003)). On the other hand, high-velocity regions in volcanic areas are generally understood in terms of intrusive solidified volumes (e.g. Taupo volcanic zone (Sherburn et al., 2003), Tunghuraua volcano (Molina et al., 2005), and Bandai volcano (Yamawaki et al., 2004)). The interpretation of Vp/Vs distributions has been addressed by several empirical and theoretical studies (e.g. Mavko, 1980; Dvorkin et al., 1999; Wang et al., 1998; Takei, 2002). The variations of Vp/Vs with pressure, temperature, composition, porosity, etc, are difficult to model. For example, both decrease and increase of Vp/Vs have been observed after a change in confining pressure, depending on depth range, presence of microcracks, fluid contents, and thermal perturbations (Nicholson and Simpson, 1985; Bonner et al., 1998; Patané et al., 2002). In spite of that, in volcanic environments high Vp/Vs values at shallow depths can be generally associated with saturated, highly fractured materials (as in Vesuvio (Scarpa et al., 2002) and Kilauea (Hansen et al., 2004)). Deep, high Vp/Vs values are rather related to bodies of partial melt (as in Etna (Patané et al., 2006), Yellowstone (Husen et al., 2004), and Long Valley (Sanders et al., 1995)). Low ratios can be also found in geothermal systems near the water–steam transition as in Yellowstone (Chatterjee et al., 1985) and Onikobe volcanic area (Nakajima and Hasegawa, 2003).

In any case, the interpretation of Vp and Vp/Vs anomalies in terms of rock properties and geological structures is generally not unique. In order to narrow down the possible interpretations and correctly understand the tomographic results, we must take into account any information available from other geological, geochemical and geophysical studies.

5.1. Interpretation of velocity anomalies

To understand the nature and meaning of the velocity anomalies depicted in Fig. 9, we are going to combine the information from the Vp and Vp/Vs models, and discuss them in the light of the results of previous studies about this region.

In the final results, the Vp distribution displays areas with low- and high-velocities, related to important lateral heterogeneities across Central São Miguel. We have revealed two low-velocity

regions around Furnas and northwest of Fogo, as well as two high-velocity regions south of Fogo and northwest of Furnas. These high-velocity anomalies might be linked through a lower velocity region.

Regarding the Vp/Vs distribution, we find two areas of low Vp/Vs ratio around Furnas and north and northeast of Fogo. A region of normal or slightly high ratio occupies the center and southwest areas (Fig. 9). In average, the Vp/Vs ratio in Central São Miguel tends to be low. The Vp/Vs ratio observed in active geothermal areas depends on the rock matrix, porosity, pore fluid content, pore pressure, temperature, and pore shape (Takei, 2002). A low Vp/Vs ratio is thought to be caused by abundance of fractures filled with boiling water. In fact, the mechanism of water–steam transition has a stronger effect on compressibility than shear modulus, leading to low Vp/Vs ratios. The relationship between low Vp/Vs ratios and geothermal areas is so sound that the study of the Vp/Vs ratio was suggested as a promising technique to identify geothermal resources and monitor their exploitation (Julian et al., 1996). Contrarily, melt inclusions reduce S-wave velocity more than P-wave velocity, resulting in high Vp/Vs ratios. Therefore, the observation of low Vp/Vs values in Central São Miguel suggests that large volumes of partial melt are not present, at least within the shallowest crust.

The seismic study by Dawson et al. (1985) estimated an average Vp/Vs value of 1.53–1.62. It is interesting to note that this value is much lower than what we find in our Vp/Vs tomography or in the preliminary work on the *e-Ruption* data by Saccorotti et al. (2004). Although, the data base and instruments are quite different, we suspect that the reduction of the Vp/Vs ratio can be a real feature. We think that the difference could be attributed to the power plant production. The continuous exploitation of the geothermal system since the 80s could have decreased the steam fraction and/or cooled the system. This could be also the origin of the observed decrease of fumarolic activity (Cruz, 2003), and general deflation of the zone (Jónsson et al., 1999).

5.1.1. Low-velocity regions

The low-velocity regions around Furnas caldera and north of Fogo volcano share a set of characteristics. Basically, they are characterized by low P-wave velocities and low Vp/Vs ratios, which decrease with depth until they reach a minimum at ∼ 2 km below sea level. Indications of low velocity in Furnas region come also from the seismic profile of Senos and Costa-Nunes (1979). They found a perturbation in the 2D velocity distribution indicating lower velocities below Furnas caldera. Results from gravity inversions (Camacho et al., 1997; Montesinos et al., 1999) indicate the presence of low-density bodies that coincide spatially with our low-velocity regions. Similar low-gravity anomalies have been related with low-density products of explosive volcanic activity and collapse processes by Sherburn et al. (2003) for Taupo zone calderas and Vanorio et al. (2005) for Campi Flegrei. Taking into account the mainly trachytic, explosive eruptive history of Fogo and Furnas volcanoes, the low-velocity anomalies may be attributed to the presence of pyroclastic products infilling the surrounding areas. These products include pumices, ignimbrite and surge deposits, phreatomagmatic ashes, and dome materials (Guest et al., 1999). However, while this explanation can be referred to the shallow layers, the continuation of the anomalies in depth may be associated with intensely fractured and/or hydrothermally altered areas (Sanders et al., 1995).

The Vp/Vs ratios are low for both of these areas. These values point to the presence of extensive steam-dominated geothermal fields. The variations of the velocity ratio with depth could be explained by changes in the fluid conditions. In the shallow part, water seems to dominate the reservoirs, producing a slightly higher

Vp/Vs ratio. The existence of thermal springs near Furnas Lake points to a shallow, liquid-dominated geothermal field, which is consistent with the higher Vp/Vs ratio observed in the first layers. The deuterium–oxygen isotope signatures indicate that the dominant fluid most likely derives from down-flow meteoric water input (Ferreira and Oskarsson, 1999). At larger depths, the sealed geothermal reservoir (Sigmundsson et al., 1995) would be filled with fluid at supercritical conditions, yielding a lower Vp and Vp/Vs ratio. This decrease in Vp/Vs ratio with depth might suggest that the fluid become steam-dominated at depths around 2 km, closer to the heat sources. The existence of vapor-filled systems at depths of about 4 km has been directly observed in wells at several geothermal fields, for example, The Geysers (Moore et al., 2001).

Therefore, a geothermal system embedded in porous, low-density pyroclastic deposits could be the origin of the low Vp, low Vp/Vs, and low-density values reported in these areas. Although the similarities point to a common explanation for the velocity anomalies in these areas around Furnas and Fogo, there are also a few differences. For example, the low-velocity area north of Fogo is much weaker. The coverage, and therefore the resolution capabilities of the tomography method, are low in this area. This can be at the origin of an underestimate of anomaly intensity.

Given this extensive geothermal activity, small amplitude, long-period seismicity of hydrothermal origin is likely to occur in Central São Miguel. In the area, long-period events and volcanic tremor, produced by the resonance of fluid-filled cavities within the volcanic medium (Chouet, 1996), have not been reported so far. The lack of noticeable volumetric, fluid-related seismic sources in Central São Miguel indicates that massive magma transport is not occurring. Nevertheless, such seismic activity might be difficult to detect without specialized instrumentation (i.e. seismic antennas) and/or adequate coverage near the geothermal areas. Recent improvement of instrumentation, with the deployment of a small aperture seismic array in the zone of Congro (A. Montalvo, personal communication) is expected to return interesting information about this kind of long-period seismic activity.

5.1.2. High-velocity regions

The high-velocity regions in Fig. 9 are distributed along a NE-SW trend, from the south of Fogo to the northwest of Furnas. These anomalies could reflect the existence, at various depths, of welded thick pyroclastic deposits, domes and more compacted material. The NE-SW trend is compatible with the direction of normal faults in the area, either inferred (Carvalho et al., 2006) or detected as electric discontinuities (Gandino et al., 1985).

The Fogo volcano could stand as a chilled remnant of a magma chamber, as described, for example, by Dawson et al. (1985). The absence of melt under the Fogo edifice is confirmed by the lack of evidence of magmatic activity from geophysical and geochemical surveys (Cruz et al., 2006). For example, there is a general subsidence in the area (Jónsson et al., 1999) and a decrease of the fumarolic system intensity (Cruz, 2003). Moreover, the magmatic input of fumarolic system is considered not as strong as to justify a direct connection between hydrothermal and magmatic activity (eRuption Working Group, 2004, and references therein).

We observe different Vp/Vs values for the two high-velocity regions. Vp/Vs span the whole range between 1.8 (in the SW high Vp anomaly) and 1.65 (in the NE high Vp). They are likely due to different phenomena and constitute an excellent example of the importance of Vp/Vs ratio to interpret information by Vp distribution. The positive Vp anomaly located in Fogo area has a high Vp/Vs ratio. This could indicate that this intrusive part is marked by low Vs, i.e. fluids contained in fractures of the medium. From this point of view, we are imaging zones of transport, advection and crystallization of fluids through a solidified intrusive. Given the strong

high-Vp anomaly, we think that water could be the fluid involved rather than melt. We guess that this fracture system represents the preferred path for up-welling of water toward the superficial geothermal fields. Something similar has been observed and explained with the presence of melt/water-saturated pathways in Etna volcano (Patané et al., 2006) and Nevado del Ruiz (Londoño and Sudo, 2002). On the other hand, the lower Vp/Vs ratio of the northeast high Vp anomaly could be due to cold volcanic material relatively unaffected by fracturing and geothermal circulation.

An intermediate region divides the two high Vp anomalies. This zone constitutes the main seismogenic region in Central São Miguel. Most of the relocated seismicity clusters here and shows a preferred NW-SE alignment (Bonagura et al., 2004; Luis, 2006). This direction dominates the tectonics of the zone also in surface geology (Guest et al., 1999; Gandino et al., 1985). Although, the constituent materials could be the same as in the neighbouring high Vp areas, the high crack density typical of faulted volumes would be at the origin of the observed lower velocity.

6. Conclusions

Our study represents a first attempt toward delineating and interpreting the subsurface seismic velocity structure of São Miguel Island. In the zone we are able to resolve, the velocity model depicts a complex picture of heterogeneities in which both Vp and Vp/Vs have large lateral contrasts over scale lengths of a few kilometres. Taking into account additional information from geophysical, geological and geochemical studies, we suggest an interpretation for the seismic velocity distribution in terms of volcanic structure. We identify pyroclastic deposits, intrusive bodies, geothermal fields, and the effects of tectonics.

In particular, we observe evidences of a vigorous geothermal field in Furnas, but not at Fogo caldera. In Fogo, everything points to the existence of the chilled remnant of a magmatic chamber, which nowadays constitutes only the pathway for water fluids. We do not find grounds for the existence of bodies of partial melt in the shallow structure.

We expect that this 3D velocity model will improve understanding of the past and present volcanic activity in Central São Miguel and the nature of the recorded seismicity. Moreover, this image could be of interest in risk evaluation and assessment for the densely inhabited areas of São Miguel.

As natural, more questions arise from the results of this seismic velocity tomography, mostly related with areas of low resolution and scale of resolved anomalies. Imaged structures could be better depicted by a wider database. At this point, long-term data from a permanent seismic network would be desirable.

References

Barberi, G., Cosentino, M.T., Gervasi, A., Guerra, I., Neri, G., Orecchio, B., 2004. Crustal seismic tomography in the Calabrian Arc region, South Italy. Phys. Earth Planet. Int. 147, 297–314.

Benz, H.M., Chouet, B., Dawson, P., Lahr, J., Page, R., Hole, J., 1996. Three-dimensional P and S wave velocity structure of Redoubt Volcano, Alaska. J. Geophys. Res. 101, 8111–8128.

Berge, P.A., Bonner, B.P., pp. UCRL-JC-144792 2002. Seismic velocities contain information about depth, lithology, fluid content and microstructure. In: Symposium on the Application of Geophysics to Engineering and Environmental Problems.

Bonagura, M.T., Damiano, N., Saccorotti, G., Ventura, G., Vilardo, G., Wallenstein, N., 2004. Fault geometries from the space distribution of earthquakes at São Miguel. Geophys. Res. Abst. 6, 07635.

Bonner, B., Roberts, J., Duba, A., Kasameyer, P., 1998. Laboratory studies of Geysers rock, and impacts on exploration. Geothermal Annual Program Review for DOE.

Buforn, E., Udías, A., Colombás, M.A., 1988. Seismicity, source mechanisms and tectonics of the Azores-Gibraltar plate boundary. Tectonophysics 152, 89–118.

Calvert, A., Sandvol, E., Seber, D., Barazangi, M., Roecker, S., Mourabit, T., Vidal, F., Alguacil, G., Jabour, N., 2000. Geodynamic evolution of the lithosphere and upper mantle beneath the Alboran region of the Western Mediterranean: Constraints from travel time tomography. J. Geophys. Res. 105, 10871–10898.

Camacho, A.G., Montesinos, F.G., Vieira, R., 1997. A three-dimensional gravity inversion applied to São Miguel, Azores. J. Geophys. Res. 102, 7705–7715.

Carvalho, M.R., Forjaz, V.H., Almeida, C., 2006. Chemical composition of deep hydrothermal fluids in the Ribeira Grande geothermal field (São Miguel, Azores). J. Volcan. Geotherm. Res. 156, 116–134.

Chatterjee, S.N., Pitt, A.M., Iyer, H.M., 1985. Vp/Vs ratios in the Yellowstone National Park region, Wyoming. J. Volcan. Geotherm. Res. 26, 213–230.

Chouet, B., 1996. Long period seismicity: its source and use in eruption forecasting. Nature 380, 309–316.

Cruz, J.V., 2003. Groundwater and volcanoes: examples from the Azores archipelago. Environ. Geol. 44, 343–355.

Cruz, J.V., Coutinho, R.M., Carvalho, M.R., Oskarsson, N., Gislason, S.R., 1999. Chemistry of waters from Furnas volcano, São Miguel, Azores: fluxes of volcanic carbon dioxide and leached material. J. Volcan. Geotherm. Res. 92, 151–167.

Cruz, J.V., Antunes, P., Amaral, C., Franca, Z., Nunes, J.C., 2006. Volcanic lakes of the Azores archipelago (Portugal: Geological setting and geochemical characterization). Mar. Geophys. Res. 20, 171–182.

Dawson, P.B., da Silva, A.R., Iyer, H.M., Evans, R., 1985. Seismic study of the Agua de Pau geothermal prospect, São Miguel, Azores. Geotherm. Res. Counc. Trans. 9 (2), 401–406.

Dawson, P.B., Chouet, B.A., Okubo, P.G., Villaseñor, A., Benz, H.M., 1999. Three-dimensional velocity structure of the Kilauea caldera, Hawaii. Geophys. Res. Lett. 26 (18), 2805–2808.

Dvorkin, J., Mavko, G., Nur, A., 1999. Overpressure detection from compressional and shear-wave data. Geophys. Res. Lett. 26, 3417–3420.

eRuption Working Group, 2004. Volcanic geology of São Miguel Island. eRuption D 3.2.2.1 report, Geological Data.

Escuer, M., 2006. Improving seismic Vp and Vs models of the Azores archipelago, Master's Thesis, University of Azores, Portugal.

Ferreira, T., Oskarsson, N., 1999. Chemistry and isotopic composition of fumarole discharges of Furnas caldera. J. Volcan. Geotherm. Res. 92, 169–179.

Finlayson, D.M., Gudmundsson, O., Itikarai, I., Nishimura, Y., Shimamura, H., 2003. Rabaul volcano, Papua New Guinea: seismic tomographic imaging of an active caldera. J. Volcan. Geotherm. Res. 124, 153–171.

Foulger, G.R., Arnott, S.K., 1993. Local Tomography: Volcanoes and the Accretionary Plate Boundary in Iceland. Chapman and Hall, London, pp. 116–134.

Gandino, A., Guidi, M., Merlo, C., Mete, L., Rossi, R., Zan, L., 1985. Preliminary model of the Ribeira Grande geothermal field (Azores Islands). Geothermics 14, 91–105.

Gongora, E., Carrilho, F., Oliveira, C., 2004. Calibration of local magnitude M_L in the Azores archipelago based on recent digital recordings. Pure Appl. Geophys. 161, 647–659.

Guest, J.E., Gaspar, J.L., Cole, P.D., Queiroz, G., Duncan, A.M., Wallenstein, N., Ferreira, T., Pacheco, J.M., 1999. Volcanic geology of Furnas Volcano, São Miguel, Azores. J. Volcan. Geotherm. Res. 92, 1–29.

Hansen, S., Thurber, C., Mandernach, M., Haslinger, F., Doran, C., 2004. Seismic Velocity and Attenuation Structure of the East Rift Zone and South Flank of Kilauea Volcano, Hawaii. Bull. Seism. Soc. Am. 94, 1430–1440.

Humphreys, E., Clayton, R.W., 1988. Adaptation of back projection tomography to seismic travel time problems. J. Geophys. Res. 93, 1073–1085.

Husen, S., Smith, R.B., Waite, G.P., 2004. Evidence for gas and magmatic sources beneath the Yellowstone volcanic field from seismic tomography imaging. J. Volcan. Geotherm. Res. 131, 397–410.

Jónsson, S., Alves, M.M., Sigmundsson, F., 1999. Low rates of deformation of the Furnas and Fogo Volcanoes, São Miguel, Azores, observed with the Global Positioning System, 1993–1997. J. Volcan. Geotherm. Res. 92, 83–94.

Julian, B.R., Ross, A., Foulger, G.R., Evans, J.R., 1996. Three-dimensional seismic image of a geothermal reservoir: the Geysers, California. Geophys. Res. Lett. 23, 685–688.

Kissling, E., Ellsworth, W.L., Eberhart-Phillips, D., Kradolfer, U., 1994. Initial reference models in local earthquake tomography. J. Geophys. Res. 99, 19635–19646.

Lees, J.M., Crosson, R.S., 1989. Tomographic inversion for three-dimensional velocity structure at Mount St. Helens using earthquake data. J. Geophys. Res. 94, 5716–5728.

Leveque, J.J., Rivera, L., Wittlinger, G., 1993. On the use of the checkerboard test to assess the resolution of tomographic inversion. Geophys. J. Int. 115, 313–318.

Lomax, A.J., Virieux, J., Volant, P., Berge, C., 2000. Probabilistic earthquake location in 3D and layered models: introduction of a Metropolis-Gibbs method and comparison with linear locations. In: Thurber, C., Rabinowitz, N. (Eds.), Advances in Seismic Event Location. Kluwer, Amsterdam, pp. 101–134.

Londoño, J.M., Sudo, Y., 2002. Velocity structure and seismic model for Nevado del Ruiz volcano (Colombia). J. Volcan. Geotherm. Res. 119, 61–87.

Lourenço, N., Miranda, J.M., Luis, J.F., Ribeiro, A., Victor, L.A.M., Madeira, J., Needham, H.D., 1998. Morpho-tectonic analysis of the Azores Volcanic Plateau from a new bathymetric compilation of the area. Mar. Geophys. Res. 20, 141–156.

Luis, J., 2006. A little insight over the recent S. Miguel seismic activity. Universidade do Algarve (http://w3.ualg.pt/~jluis/SMiguel_seismicity.htm).

Madeira, J., Ribeiro, A., 1990. Geodynamic models for the Azores triple junction: a contribution from tectonics. Tectonophysics 184, 405–415.

Masturyono, McCaffrey, R., Wark, D.A., Roecker, S.W., Fauzi, Ibrahim, G., Suckhyar, 2001. Distribution of magma beneath the Toba caldera complex, north Sumatra, Indonesia, constrained by three-dimensional P wave velocities, seismicity and gravity data. Geochem. Geophys. Geosyst. 2, 2000GC000096.

Mavko, G.M., 1980. Velocity and attenuation in partially molten rocks. J. Geophys. Res. 85, 5173–5189.

Molina, I., Kumagai, H., LePennec, J.L., Hall, M., 2005. Three-dimensional P-wave velocity structure of Tungurahua volcano, Ecuador. J. Volcan. Geotherm. Res. 147, 144–156.

Montesinos, F.G., Camacho, A.G., Vieira, R., 1999. Analysis of gravimetric anomalies in Furnas caldera, (São Miguel, Azores). J. Volcan. Geotherm. Res. 92, 67–81.

Moore, J.N., Norman, D.I., Kennedy, B.M., 2001. Fluid inclusions gas composition from an active magmatic hydrothermal system: a case study of The Geysers geothermal field, USA. Chem. Geol. 173, 3–30.

Muecke, G.K., Ade-Hall, J.M., Aumento, A., MacDonald, A., Reynolds, P.H., Hyndman, R.D., Quintino, J., Opdyke, N., Lowrie, W., 1974. Deep drilling in an active geothermal area in the Azores. Nature 252, 281–284.

Nakajima, J., Hasegawa, A., 2003. Tomographic imaging of seismic velocity structure in and around Onikobe volcanic area, Northeastern Japan: implication for fluid distribution. J. Volcan. Geotherm. Res. 127, 1–18.

Nicholson, C., Simpson, D.W., 1985. Changes in Vp/Vs with depth: implications for appropriate velocity models, improved earthquakes locations and material properties of the upper crust. BSSA 75, 1105–1123.

Ohmi, S., Lees, J.M., 1995. Three-dimensional P- and S-wave velocity structure below Unzen volcano. J. Volcan. Geotherm. Res. 65, 1–26.

Patané, D., Chiarabba, C., Cocina, O., De Gori, P., Moretti, M., Boschi, E., 2002. Tomographic images and 3D earthquake locations of the seismic swarm preceding the 2001 Mt. Etna eruption: evidence for a dyke intrusion. Geophys. Res. Lett. 29, 1497, doi:10.1029/2001GL014391.

Patané, D., Barberi, G., Cocina, O., De Gori, P., Chiarabba, C., 2006. Time-resolved seismic tomography detects magma intrusions at Mount Etna. Science 313, 821–823.

Podvin, P., Lecomte, I., 1991. Finite difference computation of traveltimes in very contrasted velocity models: a massively parallel approach and its associated tools. Geophys. J. Int. 105, 271–284.

Ritsema, J., Allen, R.M., 2003. The elusive mantle plume. Earth Planet. Sci. Lett. 207, 1–12.

Saccorotti, G., Wallenstein, N., Ibáñez, J.M., Bonagura, M.T., Damiano, N., La Rocca, M., Quadrio, A., Silva, R., Zandomeneghi, D., 2004. A seismic field survey at Fogo-Furnas volcanoes, São Miguel, Azores. Geophys. Res. Abst. 6, 04493.

Sanders, C.O., Ponko, S.C., Nixon, L.D., Schwartz, E.A., 1995. Seismological evidence for magmatic and hydrothermal structure in Long Valley caldera from local earthquake attenuation and velocity tomography. J. Geophys. Res. 100, 8311–8326.

Scarpa, R., Tronca, F., Bianco, F., Pezzo, E.D., 2002. High resolution velocity structure beneath Mount Vesuvius from seismic array data. Geophys. Res. Lett. 29, 2040, doi:10.1029/2002GL015576.

Senos, M.L., Costa-Nunes, J., 1979. Estudo da crosta nas ilhas de S. Miguel e Terceira. Resultados preliminaries. Technical report. Instituto de Meteorologia e Geofisica, Lisboa.

Sherburn, S., Bannister, S., Bibby, H., 2003. Seismic velocity structure of the central Taupo Volcanic Zone, New Zealand, from local earthquakes tomography. J. Volcan. Geotherm. Res. 122, 69–88.

Sigmundsson, F., Tryggvason, E., Alves, M.M., Alves, J.L., Palsson, K., Olafsson, H., 1995. Slow inflation of the Furnas volcano, São Miguel, Azores, suggested from initial leveling and global positioning system measurements. Geophys. Res. Lett. 22 (13), 1681–1684.

Silveira, G., Stutzmann, E., Davaille, A., Montagner, J.P., Mendes-Victor, L., Sebai, A., 2006. Azores hotspot signature in the upper mantle. J. Volcan. Geotherm. Res. 156, 23–34.

Takei, Y., 2002. Effect of pore geometry on Vp/Vs: from equilibrium geometry to crack. J. Geophys. Res. 107, doi:10.1029/2001JB00522.

Tryggvason, A., Bergman, B., 2006. A traveltime reciprocity discrepancy in the Podvin & Lecomte *time3d* finite difference algorithm. Geophys. J. Int. 165, 432–435.

Udías, A., López Arroyo, A., Mezcua, J., 1976. Seismotectonics of the Azores-Alboran region. Tectonophysics 31, 259–289.

Vanorio, T., Virieux, J., Capuano, P., Russo, G., 2005. Three dimensional seismic tomography from P wave and S wave microearthquake travel times and rock

physics characterization of the Campi Flegrei Caldera. J. Geophys. Res. 110, doi:10.1029/2004JB003102.

Villaseñor, A., Benz, H.M., Filippi, L., De Luca, G., Scarpa, R., Patané, G., Vinciguerra, S., 1998. Three-dimensional P-wave velocity structure of Mt. Etna, Italy. Geophys. Res. Lett. 25, 1975–1978.

Wang, Z., Cates, M.E., Langan, R.T., 1998. Seismic monitoring of a CO_2 flood in a carbonate reservoir: a rock physics study. Geophysics 63, 1604–1617.

Wu, H., Lees, J.M., 1999. Three-dimensional p and s wave velocity structures of the coso geothermal area, California, from microseismic travel time data. J. Geophys. Res. 104, 13217–13233.

Yamawaki, T., Tanaka, S., Ueki, S., Hamaguchi, H., Nakamichi, H., Nishimura, T., Oikawa, J., Tsutsui, T., Nishi, K., Shimizu, H., Yamaguchi, S., Miyamachi, H., Yamasato, Y., Hayashi, Y., 2004. Three-dimensional P-wave velocity structure of Bandai volcano in Northeastern Japan inferred from active seismic survey. J. Volcan. Geotherm. Res. 138, 267–282.

Zhao, D., Hasegawa, A., Horiuchi, S., 1992. Tomographic imaging of P and S wave velocity structure beneath northeastern Japan. J. Geophys. Res. 97, 19909–19928.

Zollo, A., Judenherc, S., Auger, E., D'Auria, L., Virieux, J., Capuano, P., Chiarabba, C., de Franco, R., Makris, J., Michelini, A., Musacchio, G., 2003. Evidence for the buried rim of campi flegrei caldera from 3-d active seismic imaging. Geophys. Res. Lett. 30, doi:10.1029/2003GL018173.